Characterizing the Structure and Phase Transition of Li_2RuO_3 using Variable Temperature ^{17}O and ^{7}Li NMR Spectroscopy

Philip J. Reeves[a], Ieuan D. Seymour[a, †], Kent J. Griffith[a,‡] and Clare P. Grey[*a]

[a]Department of Chemistry, University of Cambridge, Lensfield Road, Cambridge, CB2 1EW, UK.

Li-excess lithium-ion battery cathode materials and the role that reversible anionic redox may play in their high capacities, have generated significant interest, motivating studies of the oxygen local structure. Li_2RuO_3 is an intriguing Li-excess model compound, which is studied here by local (^7Li and ^{17}O MAS NMR) and long-range (X-ray and neutron diffraction) structural probes. Li_2RuO_3 is often reported as adopting the $C2/m$ or the $C/2c$ space group, which ignores the important role that Ru–Ru dimerization plays in controlling its properties. ^{17}O NMR reveals four oxygen sites confirming the room temperature $P2_1/m$ structure proposed by Miura, Y.; Yasui, Y.; Sato, M.; Igawa, N.; Kakurai, K. *J. Phys. Soc. Japan* **2007**, *76*, 033705. Through the rationalisation of the ^{17}O NMR shifts, at room temperature and through the phase transition (>260°C), detailed information concerning the electronic structure and locations of the unpaired electrons in this compound is revealed.

Introduction

To meet the energy storage needs of the developing electric vehicle industry and its requirement for increasingly higher capacity batteries, many cathode materials have been studied. $LiCoO_2$ and its analogues ($LiNi_xMn_yCo_zO_2$ and $LiNi_{0.80}Co_{0.15}Al_{0.05}O_2$, for example) are the current industry standards, these materials all adopting the same α-$NaFeO_2$ structure type, with Li and TM (TM = transition metals) arranged in layers and octahedrally coordinated by O. Since 2001, the use of Li-excess cathodes materials, in which some of the TM sites are occupied by Li, have been a potential avenue to push the capacity of the traditional layered rocksalts even further[1,2]. Exchanging TM and Li ought to reduce the number of sites available for redox during Li removal, however many Li-excess materials have shown the ability to deintercalate more Li than expected if only TM oxidation is considered. The hypothesis that O participates reversibly in the redox reaction has now been extensively studied in these materials, and related model compounds: in $Li_{1.2}Mn_{0.54}Co_{0.13}Ni_{0.13}O_2$, $Li_2Ru_{0.75}Sn_{0.25}O_3$ and $Li_{1.3}Mn_{0.4}Nb_{0.3}O_2$ for example[3–5]. The proposed redox process in these cases is distinct from the electronic processes observed on O as a result of O-TM hybridization, which cannot increase the capacity beyond the expected TM redox[6].

While the exact mechanism for oxygen redox may depend on the type of cathode material in question, two main mechanisms are reported. In one case the oxidation of O is accompanied by a shortening of the O–O interatomic distances leading to stabilization by the formation of peroxo-like species.[4,7,8] The second, which is proposed to occur in the case in which strong, directional hybridization of O–TM prevents rotation of the O p orbitals towards one another, is localized hole formation on oxygen[9–11]. Owing to the difficulty in directly observing the O redox phenomenon, along with the complexity of structures of many Li-excess compounds, [12–16], model compounds, that simplify the redox processes are essential to understanding the functioning of these materials. Li_2RuO_3, which may be written as $Li(Li_{1/3}Ru_{2/3})O_2$ to emphasize the layered structure and analogy to $LiCoO_2$, is one such model system. However, the anionic redox properties of this material cannot be fully rationalized without a full understanding of the local crystallographic and electronic structures of the starting material. This is the aim of the current study.

Li_2RuO_3 has been proposed as a useful and nominally simple model compound because of its single, well characterized, TM redox couple ($Ru^{4+} \rightarrow Ru^{5+}$) as well as it's well ordered TM layer; Ru^{4+} is arranged in a honeycomb pattern with Li^+ in the center of the hexagons (Figure 1)[17,18]. In addition to its study as a battery material, Li_2RuO_3 is of interest to the physics community as a material with unusual magnetic properties. At room temperature, Ru^{4+} lattice comprises an ordered array of dimers, Li_2RuO_3 forming a valence bond crystal (VBC)[19,20] (Figure 1b). This dimerization of the low spin $4d^4$ (S = 1) ion leads to the quenching of at least one of the unpaired spins on each Ru^{4+} and a concomitant reduction in the magnetic susceptibility[21,22]. At ~270°C Li_2RuO_3 exhibits a phase transition, evidence from a pair distribution function (PDF) analysis study showing that although dimers remain above the transitions, the dimers are disordered within the lattice and thermal fluctuations drive dynamics between different dimer pairs; this is termed a resonating valence bond (RVB) state[20,21].
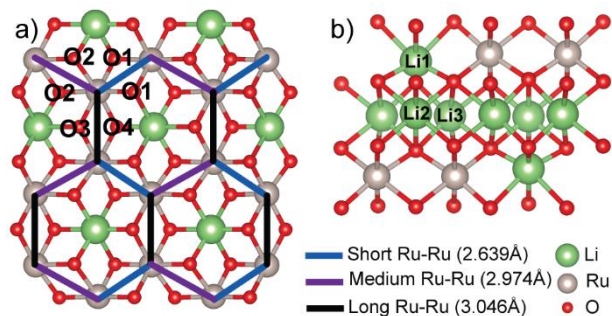
Figure 1. Schematic representation of (a) the "honeycomb" Ru layer and (b) the layered structure of Li_2RuO_3. The crystallographic O sites are labelled to show their position relative to the Ru dimers and the Li sites are shown in the position within the layers.

The structure of Li_2RuO_3 is often described as adopting the $C2/c$ unit cell, as was reported in much of the early literature[17,18,23]. Owing to the significant influence of the Ru dimerization upon the magnetism, heat capacity and resistivity, it's effect on the structure been more thoroughly explored by the physics community. Miura et al. used powder neutron diffraction to show that the structure adopts space group $P2_1/m$, in which the dimers form an "armchair" configuration at low temperatures; at high temperature the space group is $C2/m$[24]. Our own neutron diffraction study has reproduced this result, with additional peaks being observed at room temperature that are unexplained by the $C2/m$ or the $C2/c$ cell, but consistent are with $P2_1/m$ cell (section S2.1). In this study we investigate the ^7Li and ^{17}O NMR of Li_2RuO_3 through its phase transition. By careful assignment and rationalization of the NMR spectra, taking into account the dimerization, we provide insights into the structure and subtle ordering in this important compound. Given the difficulty in acquiring and interpreting the ^{17}O NMR spectra of paramagnetic materials [25,26] the current work serves as an important first step in applying this methodology to study the electrochemically cycled electrode materials.

Experimental and Theoretical Methods

Li_2RuO_3 was synthesized by solid state methods. Li_2CO_3 (Sigma Aldrich 99.997%, 10% excess) and RuO_2 (Alfa Aesar 99.9%, dried at 500 °C overnight) were ground together and heated to 600 °C for 12 hrs, then cold-pressed into pellets and heated further to 900 °C for 12 hrs and then to 1000 °C for 12 h with intermediate grinding. To record the ^{17}O NMR spectra, samples were enriched in the I = 5/2 NMR active nucleus ^{17}O, by heating the hand-ground precursors materials in a static O_2 (70% ^{17}O NUKEM Isotopes) environment at ~380 kPa at 1000 °C for 24 hrs.

Powder x-ray diffraction patterns were recorded on a Panalytical Empyrean diffractometer emitting Cu Kα (1.540598 Å + 1.544426 Å, 1:1 ratio) radiation. Scans were recorded from 5-86° 2θ in steps of 0.017° 2θ. Constant-wavelength neutron scattering measurements were performed on SPODI, the high-resolution neutron diffraction beamline at MLZ in Garching, Germany. Li_2RuO_3 was packed under air into a 10 mm diameter cylindrical sample holder made of vanadium. Rietveld refinements were performed using GSAS-II[27].

NMR experiments were conducted at various fields and MAS frequencies. The presented spectra use a rotor synchronised Hahn echo pulse sequence where the echo delay is equal to one rotor period. Full NMR acquisition parameters are given in the supplementary section S3.1.

Density functional theory (DFT) calculations were performed using the augmented planewave plus local orbital APW+lo[28,29] method in ELK[30], a linear full-potential linearized augmented plane wave (FP-LAPW) code. Additional computational details are given in supplementary section S5.1.

Results and Discussion

Li_2RuO_3 was studied by diffraction, magnetic studies and NMR spectroscopy. An effective magnetic moment, μ_{eff}, at room temperature of $0.41\mu_B$ (S4.1) was determined, consistent with previous studies confirming that the number of unpaired electrons per Ru^{4+} ion is far fewer than expected for a low-spin d^4 (S = 1) transition metal[18,31,32]. The origin of this magnetic behavior is the long-range dimerization of the Ru which gives a distorted Ru layer (Figure 1a). The value of μ_{eff} is even lower than that expected for a S=1/2 ion using the spin only formula consistent with spin-orbit coupling and/or partial coupling of both unpaired electrons (see below).

Room Temperature NMR Spectroscopy: The room temperature magic angle spinning (MAS) (60kHz) ^7Li spectrum was collected and, as observed in previous studies, there are two main resonances centered around ~27ppm and ~47ppm[33,34] (Figure 2). These environments can be modelled with three peaks in a 2:1:1 ratio. The $P2_1/m$ structure has three Li sites in the asymmetric unit: Li1 (2e) in the Ru-layer and Li2 (2e) and Li3 (4f) sites in the Li-layer (Figure 1b). We assign the peaks at 25ppm and 31ppm to Li2 and Li3 based on their similar shifts (they are both Li-layer sites) and their integrated intensities, which match what is expected from the crystal structure. The 47ppm peak is assigned to the structurally distinct Li1 site which lies in the Ru-layer.

As the paramagnetic (Fermi-contact interaction) contributions to the $^{6,7}Li$ NMR shift are relatively large, it is reasonable to assume that they are the dominant contributions to the total shift. The overall Fermi-contact interaction can often be understood using a bond pathway approach where the Fermi-contact shift is considered additive: the shift of a site being the sum of all the individual nearest neighbor and next nearest neighbor contributions. This methodology is well established for Li, particularly in the case of octahedral Li, where the sign and size of the shift can be predicted by consideration of the orbital occupation and the Li-O-M bond angle[35,36]. Regardless of the effect of the dimerization, for Ru^{4+} with localized electrons the expected shift for a 90° Ru–Li–O pathway is positive whereas for a 180° Ru–Li–O pathway it is expected to be negative[36]. Li1 has only 90° pathways to Ru^{4+} whereas Li2 and Li3 have both, therefore it is reasonable to assign the more positive shift to Li1.
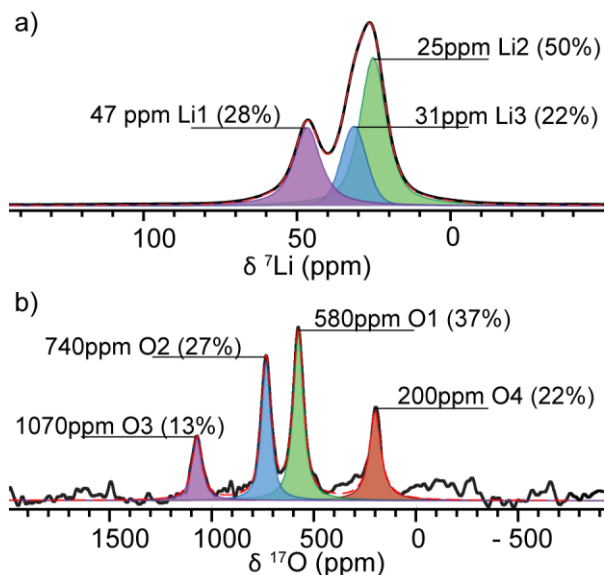
Figure 2. ^{7}Li MAS NMR (a) and ^{17}O MAS NMR spectrum (b) of Li_2RuO_3 at room temperature. Peaks fitted and labelled with their shift, assigned site and relative integrated intensity (in brackets).

The observed ^{6,7}Li shifts (and corresponding bond pathway contributions) are noticeably lower than those caused by the (S=3/2) Mn^{4+} ions in the structurally related material Li_2MnO_3, which are on the order of 750 and 1500ppm for the Li and TM layers respectively.[37] This is consistent with a reduction in the number of unpaired spins in Ru^{4+} due to dimerization, as discussed in greater detail below, and the lower magnetic susceptibility of Li_2RuO_3: for Li_2MnO_3 the effective magnetic moment is close to the spin only value of 3.85 μ_B (3.56 μ_B and 3.43 μ_B for in plane and out of plane moments respectively[38]) much larger than the measured effective moment for Li_2RuO_3 of 0.41 μ_B.

The ^{17}O NMR spectrum of ^{17}O-enriched Li_2RuO_3 displays 4 distinct O shifts at 200, 580, 740 and 1070ppm. The ratio of these shifts is approximately 1:2:2:1, which is in line with the expectation from the $P2_1/m$ crystal structure which contains four oxygen sites (Figure 1a). This is in contrast to the $C2/c$ structure which contains only 3 O sites with an expected ratio of 1:1:1. ~4% RuO_2 was observed by XRD in the enriched sample but was not observed in the NMR spectrum of this sample, presumably because of its low concentration. The ^{17}O NMR shift of RuO_2 is known (917ppm)[39] and the RuO_2 impurity can be observed in samples with a greater weight percentage of RuO_2 (S1.1).

In order to assign the ^{7}Li and ^{17}O NMR resonances of Li_2RuO_3 and provide further insight into the electronic structure and magnetic properties, first principles calculations were performed. The DFT optimized $P2_1/m$ structure previously reported by Kimber et al. [21] was first used to calculate the unpaired spin density at the nuclear positions of ^{7}Li and ^{17}O. In addition to this structure, in which the dimers are arranged in an "armchair" configuration, spin densities that result from the previously reported[21] $C2/m$ (parallel)

dimer structure and un-dimerized $C2/m$ (uniform) structure were also calculated for comparison (Figure S5.2). As discussed by Kimber et al. calculations with the $P2_1/m$ structure lead to a 0K structure with an unpaired spin density corresponding to approximately S = ½; the density of states plots qualitatively reproduce the MO diagram shown in Figure 3c but with close-to-equal occupation of the π* and δ* orbitals (see addition discussion in section S5.2), imply quasidegeneracy of these orbitals.

It is necessary to calculate a scaling factor in order to derive an ambient temperature Fermi contact shift (the paramagnetic contribution to the NMR shift), from the calculated unpaired spin densities of the 0K structure, which correspond to a perfect ferromagnetic alignment of all the unpaired spins. In most cases, the ferromagnetic ground state predicted by DFT has formal spin that is simply determined by the oxidation state of the TM ions. Here, however, due to the dimerization this is no longer trivial. As stated above, the calculated 0K structure has S=1/2 per Ru^{4+}, whereas the experimental effective moment suggests S<1/2. The experimental effective magnetic moment is used here to scale the 0K unpaired spin density (equation S3) in order to account for this. The unpaired spin densities, calculated Fermi-contact shifts and experimental shifts are compared in Table 1.

In the case of Li, each calculated structure gives unpaired spin densities, which qualitatively reproduce the experimental spectrum and the relative sizes of the shifts. I.e. The Li1 site in the $Li_{1/3}Ru_{2/3}$ layer has essentially twice the unpaired spin density of the Li2 and Li3 sites in the Li layer and the multiplicities of these sites give the observed peak ratios. The calculated unpaired spin densities are much lower for either of the dimerized structures, the fit being better for the $P2_1/m$ vs. $C2/m$ structure (which predicts a larger difference between the Li2 and Li3 shifts than seen experimentally). However, the Li NMR results do not unambiguously prove that the structure is dimerized.

In contrast, the calculated oxygen shifts can offer more insight. The magnitude of the unpaired spin density at the nuclear position of the four O sites (Table 1) in the $P2_1/m$ structure is $\rho_{o4} \leq \rho_{o1} \leq \rho_{o2} \leq \rho_{o1}$, which is in good agreement with the observed ^{17}O NMR spectrum, where we observe four peaks with the expected 1:2:2:1 intensity ratio. The $C2/m$ structures both only have two O sites and thus only two ^{17}O resonances would be expected. Although the Fermi-contact interaction generally dominates the NMR shifts of paramagnetic solids, there will also be a contribution from the chemical shift, which could be significant in the case of ^{17}O, particularly in this system where S<1/2: the ^{17}O resonances of Li_2TiO_3, which is isostructural to undimerized Li_2RuO_3, and Li_2MnO_3, have large ^{17}O chemical shifts of 372.3 and 409.8 ppm[40]. Thus, while the large differences between the shifts of the observed Li_2RuO_3 resonance are ascribed to the differences in the Fermi-contact shifts, the systematic under prediction of the experimental shifts in the DFT calculations is ascribed at least in part to the chemical shift, which on the basis of the Li_2TiO_3 shifts may contribute as much as 400 ppm to the overall shift. There is another more subtle point: on initial inspection it may appear that the magnitudes of the ^{17}O spin densities of the $C2/m$ S=1 non-dimerized structure, which are approximately

Table 1. Unpaired spin density at the ^{7}Li and ^{17}O nuclear positions from DFT calculations for the various proposed Li$_2$Ru$_2$O$_3$ structures. The calculated room temperature shift for the $P2_1/m$ structure (obtained assuming the experimentally determined magnetic susceptibilities) is compared with the experimental NMR shift values.

	Unpaired Nuclear Spin Density $1 \times 10^{-3}\rho(0)$ (1/a$_0^3$)			Calculated Fermi-contact Shift (ppm)	Observed Shift (ppm)*
Site	$P2_1/m$ (armchair)	$C2/m$ (parallel)	$C2/m$ (uniform)	$P2_1/m$ (armchair)	
Li1	3.14 (2e)	2.18 (2a)	7.23 (2a)	23	47
Li2	1.48 (4f)	0.93 (4h)	4.32 (4h)	11	25
Li3	1.71 (2e)	1.47 (2d)	4.54(2d)	13	31
O1	26.4 (4f)	33.6(8j)	76.9 (8j)	197	580
O2	47.6 (4f)	49.9 (4i)	70.3 (4i)	355	740
O3	69.9(2e)	-	-	521	1070
O4	9.4 (2e)	-	-	70	200

*Observed shift includes contributions from both the Fermi-contact and chemical shifts.

double the $P2_1$/m spin densities, might yield shifts closer to the experimental shifts. This ignores the scaling factor needed to convert the 0K structure to the room temperature Fermi-contact shift. If the predicted effective magnetic moment that arises from the S = 1 $C2/m$ structure is accounted for, this leads to predicted shifts that are much larger than the observed shifts. A similar phenomenon is responsible for the much larger Fermi contact shifts seen for the S = 3/2 Li$_2$MnO$_3$ material. The previously reported spin densities of Li$_2$MnO$_3$ are compared with those of Li$_2$RuO$_3$, highlighting the important role that the reduced susceptibility plays in the comparatively small NMR shifts of Li$_2$RuO$_3$, in section S5.2.

Further insight into the causes of the differences in the spin densities and Fermi contact shifts of the four resonances can be obtained by analyzing the structure and Ru–O/Ru–Ru bonding in more detail. The unpaired electrons in the low-spin d^4 Ru^{4+} ions are found in the t$_{2g}$ symmetry orbitals; these valence electrons are normally non-bonding in an octahedral complex but within the $P2_1/m$ dimerized structure form covalent bonds along the Ru-Ru short distances (Figure 3a), the strong σ type overlap between the d$_{xy}$ orbitals being the main driver for dimerization. This dimerization is calculated by Kimber et al. to cause a bonding-antibonding split of >2 eV[21]. This strong interaction effectively removes two unpaired electrons from the Ru–Ru pair leaving six electrons to populate the remaining orbitals. By forming appropriate linear combinations of the other t$_{2g}$ orbitals (d$_{xz}$ and d$_{yz}$) π and δ type overlaps are also possible (Figure 3c and d). If the energy gap between the π* and δ* orbitals were large enough to overcome the electron pairing energy, an S = 0 ground state would be formed with filled π, δ and π* and empty δ* orbitals. DFT calculations by other authors suggest that the π* and δ* orbitals are in fact very close in energy so that they can be considered quasidegenerate[41]. This would lead to a ground state with one unpaired elec-

tron per Ru^{4+} with the unpaired electrons primarily contained in the π* and δ* antibonding orbitals of the Ru–Ru bond. The effective magnetic moment for our sample determined of 0.41μB (S4.1) indicates that the average number of unpaired spins may be lower than one with a degree of electron pairing in the π* orbital; nonetheless, the unpaired spins will still reside in the π* and δ* orbitals.

In an undistorted octahedron the spin transfer expected from a t$_{2g}$ orbital to the M–O–Li pathway is symmetric and positive (Figure 3f)[36], however due to the dimerization and lifting of the degeneracy of the t$_{2g}$ orbitals, the t$_{2g}$ spin transfer pathway, is different for each of the Ru–O bonds and not all the t$_{2g}$ orbitals contribute equally to the spin transfer. By analogy with bonds formed in C–C molecules, the π* and δ* orbitals, which contain the most unpaired electron density, comprise lobes which mostly point away from the Ru–Ru dimers. The spatial extent of the π* and δ* orbitals is largest for the oxygen that are in the plane of and pointing away from the Ru–Ru dimer i.e. "outward" pathways (Figure 3h). Following the hypothesis that more effective overlap with the O 2p orbitals will lead to larger induced shifts, the shift caused by each pathway should increase in magnitude from smallest to largest: inward, axial, outward (Figure 3).

Table 2. Number of each type of O-Ru bond pathways for each O site.

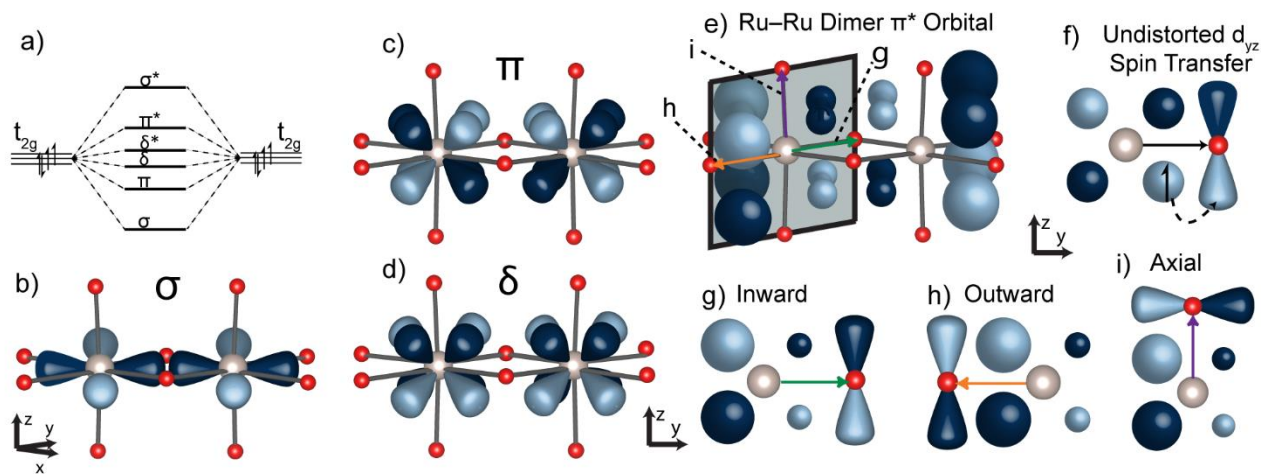| Site	Wyckoff Symbol	Number of d–p π-Type Overlaps			
		Outwards	Axial	Inwards	Inactive
O1	4f	0	0	2	2
O2	4f	1	2	0	1
O3	2e	2	0	0	2
O4	2e	0	4	0	0

Figure 3. (a) Cartoon showing the energy levels expected for a Ru–Ru dimer. (b) The strong σ-type overlap between the d_{xy} orbitals. (c) The π bonding overlap that is possible by the in-phase overlap of the π symmetry combination of the d_{xz} and d_{yz} orbitals. (d) The δ type that is possible by the in-phase overlap of the δ symmetry combination of the d_{xz} and d_{yz} orbitals; out of phase combinations give rise to the σ*, π* and δ* molecular orbitals. (e) Visualisation of the π* orbital showing the distortion of the paramagnetic electron's wavefunctions; the δ* orbital is not shown but would have qualitatively identical shape. (f) Schematic of spin transfer from a partially occupied t_{2g} d orbital to the O 2p orbital: The M and O orbitals are of the correct symmetry to form a spin orbital and hence the polarisation of the t_{2g} electron is transfer to the whole M–O pathway giving a positive shift. (g), (h) and (i) show the effect of the distortion on the spin transfer pathways for each of the possible Ru–O bonds.

Each oxygen site has two Ru neighbors and for each Ru neighbor each oxygen has two p orbitals of the correct symmetry to form p–d π pathways. As the d_{xy} orbital forms the σ bond of the dimer it does not contribute to the hyperfine shift. By examining the connectivity of the four sites (Table 2) and considering their relative intensities it is possible to rationalize the magnitude of each of the observed shifts. O3 is a 2e Wyckoff site with the most outwards pathways (Table 2) and so is assigned to the peak at 1070ppm. O2 has the next most outwards pathways and is a 4f site, consistent with the greater intensity of the 740ppm peak. The second 4f site (O1) is assigned to the 580ppm peak and finally O4 is assigned to the 200ppm peak. These assignments are consistent with the DFT calculations.

Variable Temperature NMR Studies: The phase transition in Li_2RuO_3 can be probed using variable temperature NMR. In the case of both the ^{7}Li and ^{17}O NMR spectra, the peaks move to higher shifts on increasing the temperature; this is contrary to what is normally observed for Fermi-contact shifts of paramagnetic systems in the Curie-Weiss regime, where a decrease in shift with temperature is generally seen. In the initial stage of heating, this can be ascribed to the increase in the number of unpaired spins before the phase transition due to thermal fluctuations and the increased occupations of higher energy δ* states; in the magnetometry data the susceptibility rises slightly above 300K (S4.1). Above the phase transition the sharp rise in the susceptibility is accompanied by a sharp increase in the size of the observed shifts as expected[22].

In the case of [7]Li, the signal is lost as the critical temperature (of the phase transition) is reached. This is attributed to fluctuations, either electronic or magnetic, on the NMR timescale that occur at the onset of the phase transition and which cause very rapid spin-spin (T_2) and/or spin-lattice (T_1) relaxation such that coherence is lost during the echo delay. A similar loss of [7]Li signal has been observed in partially delithiated $LiCoO_2$ and low TM content NMCs before they undergo their metal-insulator transitions.[42,43] Here the loss of signal was proposed to be due to localised and isolated Co^{4+} ions that cause very fast relaxation of the Li nuclear spins via a very efficient hyperfine transfer from the t_{2g} 3d electrons, which point directly at the Li 2s orbitals, to the Li. A similar mechanism may be responsible for the loss of signal in Li_2RuO_3. As the critical temperature is approached and the dimers increasingly break up, more localised and unpaired 4d t_{2g} electrons are formed. Rapid nuclear relaxation is caused by slow electronic relaxation times (T_{1e}s) of these unpaired electrons on the timescale of the electron-nuclear coupling. As the temperature increases, the fluctuations increase, the T_{1e}s decrease, (the system becomes increasingly paramagnetic) and the nuclear relaxation times increase and Li signal is again observed. Unfortunately, due to hardware constraints, the MAS frequency attainable at very high temperatures is quite low, which hinders unambiguous assignment of the isotropic resonances. On the basis of the high temperature structure reported by Miura et al.[24] which has three Li sites which are broadly similar to the room temperature structure, our tentative assignment is that two similar resonances occur at ~135ppm (Li in the Li layer) and a second broader resonance is present from 300-500ppm (Li in the TM layer). Details of these assignments are in supplementary section S3.2.
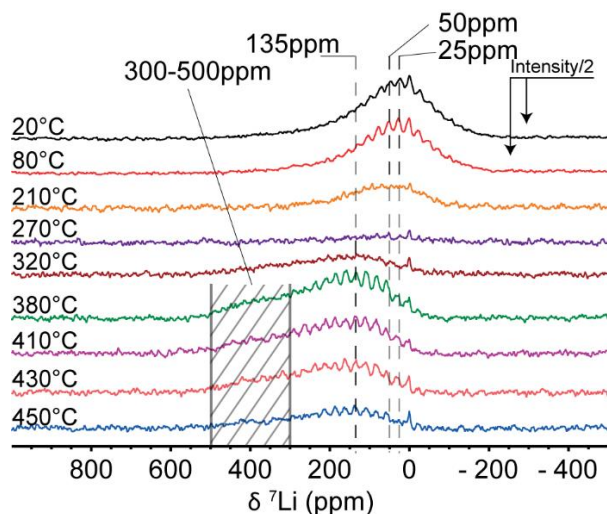
Figure 4. High temperature ^{7}Li NMR spectra of Li$_2$RuO$_3$. Isotropic resonances are indicated; the additional peaks are spinning sidebands. The hashed area indicates the region in which the second peak in the high temperature spectra is expected but for which no sharp resonance is observed.

Although broadening of the ^{17}O resonances is seen at the phase transition and above, they never vanish completely and the spectra were more easily acquired and the shifts tracked through the phase transition (Figure 5). Using variable offset cumulative spectra (VOCS) collected with an automatic tuning/matching robot[44], the full bandwidth of the spectrum of the more strongly paramagnetic oxygen can be captured. At 220°C, before the onset of the phase transition there are two isotropic ^{17}O resonances at ~1180ppm and ~820ppm. These evolve steadily to 1500ppm and 1100ppm respectively, at 260°C. These intermediate temperature spectra are more typical of paramagnetic O and the broadening points to a loss in the distinct identities of the O sites as the phase transition approaches along with broadening due to increased T$_{1e}$s of the Ru 4d electrons. Above the phase transition, the resonances shift further to ~2300ppm and ~2150ppm and broad manifold of well resolved spinning sidebands are observed. Although the calculated un-dimerized 'uniform' structure is not a good representation of the true high temperature structure, which is an intrinsically dynamic system in which short Ru–Ru distances persist, it can give some insight into the assignment of the high temperature NMR. Without calculating the shifts, qualitative comparison of the unpaired spin densities suggest that the peaks can be assigned to the two oxygen sites with Wyckoff positions 8j (~2300ppm) and 4i (~2150ppm) in the high temperature C/2m structure. This is in agreement with the relative magnitudes of the shifts for 8j and 4i sites in Li$_2$MnO$_3$.[25] Additional discussion of this assignment can be found in supplementary section S3.3. The presence of only two resonances suggests that the average local structure experienced by the O is consistent with the C/2m structure and that the dimerisation above the transition is dynamically averaged on the NMR time scale.
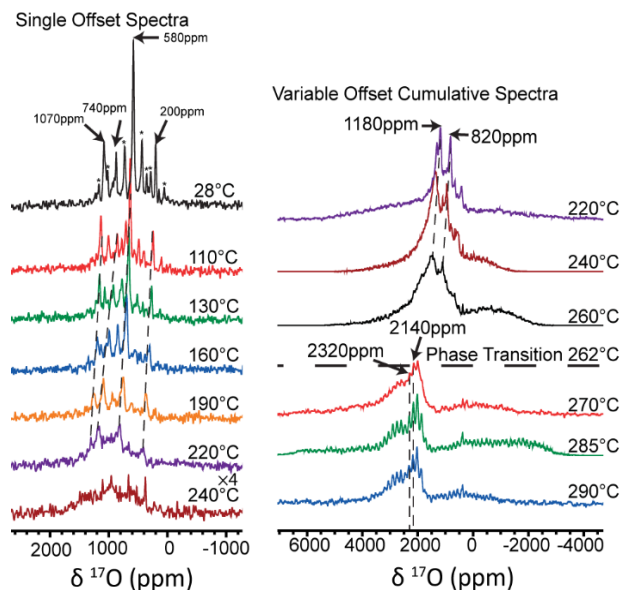

Figure 5. High temperature MAS NMR ^{17}O spectra of Li$_2$RuO$_3$. Isotropic resonances and their evolution with temperature are labelled with dashed lines. Other peaks are spinning sidebands. Single offset spectra are recorded with a quantitative recycle delay (75ms). The T$_1$ is reduced as the temperature rises so the variable offset spectra were recorded using a shorter but still quantitative recycled delay (5ms).

That more significant broadening seen for ^{7}Li rather than ^{17}O is tentatively ascribed to the orientation of the t$_{2g}$ orbitals which point directly towards Li but not towards O, allowing a direct overlap with the Li 2s orbitals. It also likely that the ^{17}O relaxation (and thus broadening) depends more sensitively on which orbitals are involved (since the Li ions are coordinated to multiple oxygen atoms). Interestingly the 740ppm peak (O2) has the shortest spin-lattice relaxation (T$_1$) (10ms vs ~200ms for the other sites) at room temperature and has a steeper rise in shift with temperature. The reason for this may lie in the nature of the thermal fluctuations that lead to the phase transition. Each O site has only one Ru(t$_{2g}$)–O(2p)–Ru(t$_{2g}$) connection which plays a role in the magnetic interactions between the Ru^{4+} ions, O2 joins the strongly bonded and spin paired σ orbital of one Ru^{4+} to partially spin unpaired π* and δ* orbitals on a second Ru^{4+}, whereas the other O sites link orbitals with the same occupation (i.e. σ↔σ and π*/δ*↔π*/δ*). This unique connectivity may cause O2 to be more sensitive to an increase in the number of unpaired spins and changes in their electronic relaxation times, induced by the thermal excitations.

Implications for battery chemistry: We now briefly consider the effect of the dimerization in Li$_2$RuO$_3$ on its electrochemical performance in a lithium-ion battery. Ignoring any effect of Li removal on the structure and considering only the Ru^{4+}→Ru^{5+} oxidation that accompanies the first plateau observed electrochemically (~3.6V vs. Li)[4], it might be expected that oxidation might result in stronger Ru–Ru bonds, since electrons are removed from the antibonding π*/δ* orbitals. This is consistent with prior work of other authors that has shown that, at least in the case of chemical delithiation, the Ru–Ru dimerization is preserved and the magnetic susceptibility is reduced, upon removal of 0.73Li per

formula unit [45]. One proposed mechanism for anionic redox in the 4/5d transition metal cathodes relies on a rearrangement of the oxygen sublattice at high potentials, leading to stabilization of $O_2^{3-/2-}$ in peroxo-like dimers[4,8,9]. If the structure contains Ru–Ru dimers, this affects the Ru–O bonding (as discussed above) and the Ru–O bond lengths. This will affect both the potential reordering of the oxygen sub-lattice, and also the ionic character of the oxygen anions; the latter is significant as, in the second mechanism proposed to explain oxygen redox,[6,10] the more ionic anions are the ones which are proposed to be oxidized at lower potentials. The full effect of the dimerization on the electrochemistry of Li_2RuO_3 will be the subject of a future work.

Conclusions

In summary, the nature of the local structure and phase transition in Li_2RuO_3 have been determined from ^7Li and ^{17}O NMR supported by density functional theory, bonding analysis, and neutron diffraction. These data confirm that the room temperature structure contains four distinct O sites; this is in good agreement with the previously reported but often overlooked $P2_1/m$ structure and our DFT computed shifts. The size of the O hyperfine shifts can be rationalized when the Ru dimerization is accounted for: simple bond pathway analyses, typically used to analyze the spectra of paramagnetic materials, are not sufficient[36]; instead the effect of metal-metal bonding on the Ru–O overlap needs to be considered. Careful analysis of both the spin densities and magnetic susceptibilities is required in order to make accurate predictions of hyperfine shifts. The much larger hyperfine shifts observed above the transition temperature for both nuclei show that the unpaired electron density expected on Ru^{4+} is largely quenched in the room temperature structure. Of note, by comparing the experimental and DFT-derived results we show that although the unpaired spin densities seen for Li_2RuO_3—even in the dimerized state—are larger than those of the related material Li_2MnO_3, despite the fewer numbers of unpaired spins, the susceptibility of Li_2MnO_3 results in a noticeably larger hyperfine shifts at room temperature.

It is common practice to use shifts derived from model compounds such as Li_2RuO_3 to help rationalize spectra of other compounds of interest for example Sn doped and delithiated Li_2RuO_3. Here we demonstrated that the room temperature structure of pristine Li_2RuO_3 may not always be the most appropriate model compound with which to help rationalize the NMR spectra of Ru^{4+} substituted materials: a more careful analysis of how substitution affects long range ordering is required. The high temperature phase may provide a more appropriate model for this type of analysis and we hope that the shifts observed here will prove useful in interpreting spectra from other systems and samples relevant to understanding the electrochemical functioning of these materials. The extension of the highly versatile bond pathway approach to rationalize the NMR shifts of ^{17}O is a significant step towards using this challenging nucleus effectively to understand delithiated Li-ion battery cathodes, which is a development that is highly anticipated by the battery community. Our results highlight that TM-TM interactions should not be ignored in the case of 4d and 5d TM containing compounds, particularly in the case of anionic redox

cathode materials, as their effects on the oxygen lattice are non-trivial.

ASSOCIATED CONTENT

Supporting Information
Additional details of ^{17}O enrichment, further NMR and diffraction conditions, magnetic measurements, computational methods and results and NMR assignments

AUTHOR INFORMATION

Corresponding Author
* Email: cpg27@cam.ac.uk

Present Addresses

† *Current address: Department of Chemistry and the Institute for Computational Engineering and Sciences, The University of Texas at Austin, 105 East 24th Street, Stop A5300, Austin, Texas 78712, United States*

‡ *Current address: Northwestern University, Department of Materials Science and Engineering*
2200 Campus Drive
Cook 2036
Evanston, IL, USA 60208

Author Contributions

The manuscript was written through contributions of all authors. NMR, synthesis and characterization carried out by PJR, Calculations performed by IDS, Neutron diffraction performed by KJG. Supervision and direction from CPG.

Notes
The authors declare no competing financial interest

REFERENCES

(1) Lu, Z.; MacNeil, D. D.; Dahn, J. R. Layered Cathode Materials Li[Ni$_x$Li$_{(1/3-2x/3)}$Mn$_{(2/3-x/3)}$]O$_2$ for Lithium-Ion Batteries. *Electrochem. Solid-State Lett.* **2001**, *4*, A191.

(2) Ohzuku, T.; Makimura, Y. Layered Lithium Insertion Material of LiNi$_{1/2}$Mn$_{1/2}$O$_2$: A Possible Alternative to LiCoO$_2$ for Advanced Lithium-Ion Batteries. *Chem. Lett.* **2001**, *2*, 744–745.

(3) Koga, H.; Croguennec, L.; Ménétrier, M.; Douhil, K.; Belin, S.; Bourgeois, L.; Suard, E.; Weill, F.; Delmas, C. Reversible Oxygen Participation to the Redox Processes Revealed for A792.

(4) Sathiya, M.; Rousse, G.; Ramesha, K.; Laisa, C. P.; Vezin, H.; Sougrati, M. T.; Doublet, M.-L.; Foix, D.; Gonbeau, D.; Walker, W.; et al. Reversible Anionic Redox Chemistry in High-Capacity Layered-Oxide Electrodes. *Nat. Mater.* **2013**, *12*, 827–835.

(5) Yabuuchi, N.; Takeuchi, M.; Nakayama, M.; Shiiba, H.; Ogawa, M.; Nakayama, K.; Ohta, T.; Endo, D.; Ozaki, T.; Inamasu, T.; et al. High-Capacity Electrode Materials for Rechargeable Lithium Batteries: Li_3NbO_4 Based System with Cation-Disordered Rocksalt Structure. *Proc. Natl. Acad. Sci. U. S. A.* **2015**, *112*, 7650–7655.

(6) Seo, D.; Lee, J.; Urban, A.; Malik, R.; Kang, S.; Ceder, G. The Electronic Origin of the Oxygen Redox Activity in Li-Excess Cathode Materials. *Nat. Chem.* **2016**, *10.1038/NC*, 1–6.

(7) Saubanere, M.; McCalla, E.; Tarascon, J.-M.; Doublet, M.-L. The Intriguing Question of Anionic Redox in High-Energy Density Cathodes for Li-Ion Batteries. *Energy Environ. Sci.* **2016**, 984–991.

(8) McCalla, E.; Abakumov, A. M.; Saubanère, M.; Foix, D.; Berg, E. J.; Rousse, G.; Doublet, M.-L.; Gonbeau, D.; Novák, P.; Van Tendeloo, G.; et al. Visualization of O-O Peroxo-like Dimers in High-Capacity Layered Oxides for Li-Ion Batteries. *Science* **2015**, *350*, 1516–1521.

(9) Seo, D. H.; Lee, J.; Urban, A.; Malik, R.; Kang, S.; Ceder, G. The Structural and Chemical Origin of the Oxygen Redox Activity in Layered and Cation-Disordered Li-Excess Cathode Materials. *Nat. Chem.* **2016**, *8*, 692–697.

(10) Luo, K.; Roberts, M. R.; Hao, R.; Guerrini, N.; Pickup, D. M.; Liu, Y.-S.; Edström, K.; Guo, J.; Chadwick, A. V.; Duda, L. C.; et al. Charge-Compensation in 3d-Transition-Metal-Oxide Intercalation Cathodes through the Generation of Localized Electron Holes on Oxygen. *Nat. Chem.* **2016**.

(11) Koga, H.; Croguennec, L.; Ménétrier, M.; Mannessiez, P.; Weill, F.; Delmas, C. Different Oxygen Redox Participation for Bulk and Surface: A Possible Global Explanation for the Cycling Mechanism of $Li1.20Mn0.54Co0.13Ni0.13O2$. *J. Power Sources* **2013**, *236*, 250–258.

(12) Lu, Z.; Beaulieu, L. Y.; Donaberger, R. a.; Thomas, C. L.; Dahn, J. R. Synthesis, Structure, and Electrochemical Behavior of $Li[Ni[Sub x]Li[Sub 1/3−2x/3]Mn[Sub 2/3−x/3]]O[Sub 2]$. *J. Electrochem. Soc.* **2002**, *149*, A778.

(13) Lu, Z.; Chen, Z.; Dahn, J. R. Lack of Cation Clustering in $Li[Ni_xLi_{1/3-2x/3}Mn_{2/3-x/3}]O_2(0 < x ≤ 1/2)$ and $Li[Cr_xLi_{(1-x)/3}Mn_{(2-2x)/3}]O_2(0 < x < 1)$. *Chem. Mater.* **2003**, *15*, 3214–3220.

(14) Pan, C.; Lee, Y. J.; Ammundsen, B.; Grey, C. P. ^6Li MAS NMR Studies of the Local Structure and Electrochemical Properties of Cr-Doped Lithium Manganese and Lithium Cobalt Oxide Cathode Materials for Lithium-Ion Batteries. *Chem. Mater.* **2002**, *14*, 2289–2299.

(15) Ammundsen, B.; Paulsen, J.; Davidson, I.; Liu, R.-S.; Shen, C.-H.; Chen, J.-M.; Jang, L.-Y.; Lee, J.-F. Local Structure and First Cycle Redox Mechanism of Layered $Li[1.2]Cr[0.4]Mn[0.4]O2$ Cathode Material. *J. Electrochem. Soc.* **2002**, *149*, A431.

(16) Shukla, A. K.; Ramasse, Q. M.; Ophus, C.; Duncan, H.; Hage, F.; Chen, G. Unravelling Structural Ambiguities in Lithium- and Manganese-Rich Transition Metal Oxides. *Nat. Commun.* **2015**, *6*, 8711.

(17) Kobayashi, H.; Kanno, R.; Kawamoto, Y.; Tabuchi, M.; Nakamura, O.; Takano, M. Structure and Lithium Deintercalation of $Li_{2-x}RuO_3$. *Solid State Ionics* **1995**, *82*, 25–31.

(18) James, A. C. W. P.; Goodenough, J. B. Structure and Bonding in Lithium Ruthenate, Li_2RuO_3. **1988**, *294*, 287–294.

(19) Park, J.; Tan, T.-Y.; Adroja, D. T.; Daoud-Aladine, A.; Choi, S.; Cho, D.-Y.; Lee, S.-H.; Kim, J.; Sim, H.; Morioka, T.; et al. Robust Singlet Dimers with Fragile Ordering in Two-Dimensional Honeycomb Lattice of Li_2RuO_3. *Sci. Rep.* **2016**, *6*, 25238.

(20) Jackeli, G.; Khomskii, D. I. Classical Dimers and Dimerized Superstructure in an Orbitally Degenerate Honeycomb Antiferromagnet. *Phys. Rev. Lett.* **2008**, *100*, 1–4.

(21) Kimber, S. A. J.; Mazin, I. I.; Shen, J.; Jeschke, H. O.; Streltsov, S. V.; Argyriou, D. N.; Valentí, R.; Khomskii, D. I. Valence Bond Liquid Phase in the Honeycomb Lattice Material Li_2RuO_3. *Phys. Rev. B - Condens. Matter Mater. Phys.* **2014**, *89*, 1–5.

(22) Miura, Y.; Yasui, Y.; Sato, M.; Igawa, N.; Kakurai, K. New-Type Phase Transition of Li_2RuO_3 with Honeycomb Structure. *J. Phys. Soc. Japan* **2007**, *76*, 2–5.

(23) Dulac, J.-F. Synthese et Structure Cristallographique Du Complexe Ternaire Nouveau Li_2RuO_3. *C. R. Acad. Sc. Paris.* **1970**, *270*, 223.

(24) Miura, Y.; Sato, M.; Yamakawa, Y.; Habaguchi, T.; Ōno, Y. Structural Transition of Li_2RuO_3 Induced by Molecular-Orbit Formation. *J. Phys. Soc. Japan* **2009**, *78*, 094706.

(25) Seymour, I. D.; Middlemiss, D. S.; Halat, D. M.; Trease, N. M.; Pell, A. J.; Grey, C. P. Characterizing Oxygen Local Environments in Paramagnetic Battery Materials via ^{17}O NMR and DFT Calculations. *J. Am. Chem. Soc.* **2016**, *138*, 9405–9408.

(26) Halat, D. M.; Dervişoğlu, R.; Kim, G.; Dunstan, M. T.; Blanc, F.; Middlemiss, D. S.; Grey, C. P. Probing Oxide-Ion Mobility in the Mixed Ionic–Electronic Conductor La2 $NiO4+δ$ by Solid-State 17O MAS NMR Spectroscopy. *J. Am. Chem. Soc.* **2016**, *138*, 11958–11969.

(27) Toby, B. H.; Von Dreele, R. B. GSAS-II: The Genesis of a Modern Open-Source All Purpose Crystallography Software Package. *J. Appl. Crystallogr.* **2013**, *46*, 544–549.

(28) Singh, D. J.; Nordström, L. *Planewaves, Pseudopotentials and the LAPW Method*, 2nd ed.; Springer US: New York, 2006.

(29) Nordström, L.; Madsen, G. K. H.; Blaha, P.; Schwarz, K.; Sjöstedt, E. Efficient Linearization of the Augmented Plane-Wave Method. *Phys. Rev. B - Condens. Matter Mater. Phys.* **2001**, *64*, 1–9.

(30) The Elk Code. http://elk.sourceforge.net/ (accessed Mar 8, 2019).

(31) Wang, J. C.; Terzic, J.; Qi, T. F.; Ye, F.; Yuan, S. J.; Aswartham, S.; Streltsov, S. V.; Khomskii, D. I.; Kaul, R. K.; Cao, G. Lattice-Tuned Magnetism of $Ru^{4+}(4d^4)$ Ions in Single Crystals of the Layered Honeycomb Ruthenates Li_2RuO_3 and Na_2RuO_3. *Phys. Rev. B - Condens. Matter Mater. Phys.* **2014**, *90*, 1–6.

(32) Miura, Y.; Yasui, Y.; Sato, M.; Igawa, N.; Kakurai, K. New-Type Phase Transition of Li_2RuO_3 with Honeycomb Structure. *J. Phys. Soc. Japan* **2007**, *76*, 033705.

(33) Salager, E.; Sarou-Kanian, V.; Sathiya, M.; Tang, M.; Leriche, J.-B.; Melin, P.; Wang, Z.; Vezin, H.; Bessada, C.; Deschamps, M.; et al. Solid-State NMR of the Family of Positive Electrode Materials $Li_2Ru_{1-y}Sn_yO_3$ for Lithium-Ion Batteries. *Chem. Mater.* **2014**, *26*, 7009–7019.

(34) Arapova, I. Y.; Buzlukov, A. L.; Germov, A. Y.; Mikhalev, K. N.; Tan, T.-Y.; Park, J.-G.; Streltsov, S. V. Magnetic Properties of Li_2RuO_3 as Studied by NMR and LDA+DMFT Calculations. *JETP Lett.* **2017**, *105*, 375.

(35) Grey, C. P.; Dupré, N. NMR Studies of Cathode Materials for Lithium-Ion Rechargeable Batteries. *Chem. Rev.* **2004**, *104*, 4493–4512.

(36) Carlier, D.; Ménétrier, M.; Grey, C.; Delmas, C.; Ceder, G. Understanding the NMR Shifts in Paramagnetic Transition Metal Oxides Using Density Functional Theory Calculations. *Phys. Rev. B* **2003**, *67*, 1–14.

(37) Bréger, J.; Jiang, M.; Dupré, N.; Meng, Y. S.; Shao-Horn, Y.; Ceder, G.; Grey, C. P. High-Resolution X-Ray Diffraction, DIFFaX, NMR and First Principles Study of Disorder in the Li_2MnO_3 $Li[Ni_{1/2}Mn_{1/2}]O_2$ Solid Solution. *J. Solid State Chem.* **2005**, *178*, 2575–2585.

(38) Lee, S.; Choi, S.; Kim, J.; Sim, H. Antiferromagnetic Ordering in Li_2MnO_3 Single Crystals with a Two-Dimensional Honeycomb Lattice. *J. Phys. Condens. Matter* **2012**, *24*, 456004.

(39) Hu, Y. Y.; Liu, Z.; Nam, K. W.; Borkiewicz, O. J.; Cheng, J.; Hua, X.; Dunstan, M. T.; Yu, X.; Wiaderek, K. M.; Du, L. S.; et al. Origin of Additional Capacities in Metal Oxide Lithium-Ion Battery Electrodes. *Nat. Mater.* **2013**, *12*, 1130–1136.

(40) Bastow, T. J.; Dirken, P. J.; Smith, M. E.; Whitfield, H. J. Factors Controlling the ^{17}O NMR Chemical Shift in Ionic Mixed Metal Oxides. *J. Phys. Chem.* **1996**, *100*, 18539–18545.

(41) Johannes, M. D.; Stux, A. M.; Swider-Lyons, K. E. Electronic Structure and Properties of Li-Insertion Materials: Li_2RuO_3 and RuO_2. *Phys. Rev. B - Condens. Matter Mater. Phys.* **2008**, *77*, 075124.

(42) Ménétrier, M.; Saadoune, I.; Levasseur, S.; Delmas, C. The

Insulator–metal Transition upon Lithium Deintercalation from LiCoO2 : Electronic Properties and 7Li NMR Study. *J. Mater. Chem.* **1999**, *9*, 1135–1140.

(43)   Zeng, D.; Cabana, J.; Yoon, W. S.; Grey, C. P. Investigation of the Structural Changes in Li[NiyMn YCO(1-2y)]O2 (y = 0.05) upon Electrochemical Lithium Deintercalation. *Chem. Mater.* **2010**, *22*, 1209–1219.

(44)   Pecher, O.; Halat, D. M.; Lee, J.; Liu, Z.; Griffith, K. J.; Braun, M.; Grey, C. P. Enhanced Efficiency of Solid-State NMR Investigations of Energy Materials Using an External Automatic Tuning/Matching (EATM) Robot. *J. Magn. Reson.* **2017**, *275*, 127–136.

(45)   Jimenez-Segura, M. P.; Ikeda, A.; Kimber, S. A. J.; Giacobbe, C.; Yonezawa, S.; Maeno, Y. Effect of Delithiation on the Dimer Transition of the Honeycomb-Lattice Ruthenate $Li_{2-x}RuO_3$. *Phys. Rev. B* **2016**, *94*, 1–8.